

Subspace Prototype Guidance for Mitigating Class Imbalance in Point Cloud Semantic Segmentation

Jiawei Han¹, Kaiqi Liu^{1*}, Wei Li¹, and Guangzhi Chen²

¹ Beijing Institute of Technology

² Beihang University

Abstract. Point cloud semantic segmentation can significantly enhance the perception of an intelligent agent. Nevertheless, the discriminative capability of the segmentation network is influenced by the quantity of samples available for different categories. To mitigate the cognitive bias induced by class imbalance, this paper introduces a novel method, namely subspace prototype guidance (**SPG**), to guide the training of segmentation network. Specifically, the point cloud is initially separated into independent point sets by category to provide initial conditions for the generation of feature subspaces. The auxiliary branch which consists of an encoder and a projection head maps these point sets into separate feature subspaces. Subsequently, the feature prototypes which are extracted from the current separate subspaces and then combined with prototypes of historical subspaces guide the feature space of main branch to enhance the discriminability of features of minority categories. The prototypes derived from the feature space of main branch are also employed to guide the training of the auxiliary branch, forming a supervisory loop to maintain consistent convergence of the entire network. The experiments conducted on the large public benchmarks (i.e. S3DIS, ScanNet v2, ScanNet200, Toronto-3D) and collected real-world data illustrate that the proposed method significantly improves the segmentation performance and surpasses the state-of-the-art method. The code is available at <https://github.com/Javion11/PointLiBR.git>.

Keywords: Point cloud · Class imbalance · Subspace prototype

1 Introduction

Point cloud semantic segmentation assigns semantic labels to points within 3D data to enhance the perception, and has diverse applications in many fields like autonomous driving, robotics, and augmented reality. The development trends in point cloud semantic segmentation have focused on improving the robustness and accuracy of segmentation algorithms through the utilization of deep learning architectures [12, 22, 30, 31, 49, 57]. The remarkable endeavors dedicated

* Corresponding author, liukaiqi@bit.edu.cn

to improving network architectures have led to substantial advancements in the performance of point cloud segmentation. Some other works aim to address novel challenges with specific training and testing paradigms, such as few-shot [58] and weakly-supervised [52, 55].

However, these discriminative networks have not taken the detrimental impact of class imbalance into consideration. The categories with more training samples tend to get better segmentation accuracy. Conversely, if there are not sufficient training samples of certain categories, the high-dimensional abstract features of these categories will be obscured within the majority categories. Although oversampling [3] minority categories or undersampling [26] majority categories can balance the training samples of different categories, processing data with such a brute-force way in point cloud segmentation will compromise scene integrity and disrupt the distribution of data. Another common method for class imbalance is to balance the contributions of samples to the backpropagation gradient by adjusting the loss function, such as Focal Loss [23] and Weighted Cross-Entropy(CE) Loss [2]. Unfortunately, these methods exhibit limited improvements when applied to the task of point cloud semantic segmentation.

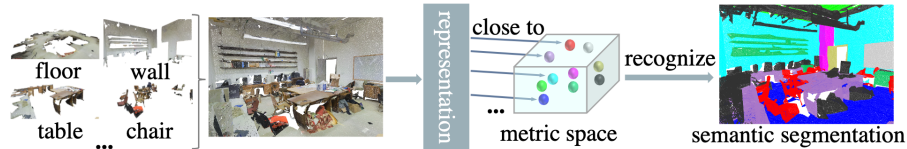


Fig. 1: Semantic understanding of **SPG**. The input point cloud is abstracted into high-dimensional features through a representation network. Then these features are assigned the corresponding category labels, which belong to the closest prototypes in the metric space.

To abstract away from the concept of sample quantities, points of the same category are regarded to share inherent uniformity in the subspace prototype guidance (**SPG**) method, specifically in the sense that their descriptions in the high-dimensional feature space are akin [39] as shown in Fig. 1. When some points are far away from their category prototypes after passing through the representation network, these points are often misclassified into incorrect categories. Therefore, **SPG** utilizes instance-balanced sampling to ensure scene integrity and facilitate the learning of improved representation networks [16]. It also employs category prototypes to narrow the intra-class variance in the feature space of the segmentation network, which helps separate the features of minority category from those of majority category. Consequently, it enhances the discrimination of minority category features and facilitates the correct classification by the classifier.

Since the point sets of different categories coexist in the scene, the features belonging to the categories with few samples tend to be overshadowed in the

features belonging to the categories with many samples, which makes it challenging to obtain accurate feature prototypes. **SPG** utilizes an auxiliary branch composed of an encoder and a projection head to separately process the features of the specific category, which is beneficial to extract the prototypes of minority categories. Furthermore, to prevent the overlap or interference of inter-class features, the input point clouds of the auxiliary branch are preprocessed by grouping them based on their categories. It can separate the mixed feature space, which effectively extracts homogeneous features and mitigates the influence of heterogeneous contextual information.

The prototype for each category contains information exclusively from points of the same category after the grouping process. **SPG** widens the distance between heterogeneous features through the loss constraint [17] to increase the discrimination of the corresponding prototypes. Prototypes containing historical scene information exhibit increased robustness to scene variations. Therefore, prototypes are updated with momentum [5, 14] to retain their ability to recognize different scenes, rather than relying solely on the information of current scene.

In addition to employing prototypes from the auxiliary branch to guide the training of the main segmentation network, the feature space of the auxiliary branch is also supervised by the correctly classified features from the main branch. The two branches mutually constrain each other and undergo joint online training, which ensures alignment in the convergence direction of the overall network. The main contributions of this work can be summarized as follows:

- This work analyzes the distribution of the features in the point cloud semantic segmentation network and introduces to use point cloud category prototypes as convergence targets to constrain the feature representation of the segmentation network.
- A novel method for extracting point cloud prototypes is proposed, which uses a plug-and-play branch consisting of an encoder and a projection head. This branch projects class-grouped point clouds into separate feature subspaces and extracts prototypes that are not interfered by other categories.
- The proposed method **SPG** utilizes prototypes from separate subspaces to guide the training of segmentation network. It significantly mitigates the negative impact of class imbalance on point cloud semantic segmentation without increasing the computational overhead during inference.

2 Related Work

This paper mitigates class imbalance in point cloud semantic segmentation with the point cloud prototype extracted from separate subspaces. We briefly review recent works on point cloud semantic segmentation, class imbalance, and category prototype.

Point cloud semantic segmentation. Compared to traditional non-learning-based approaches, deep learning-based methods [22, 30, 31, 44, 49, 50, 57] have elevated

the performance of semantic segmentation to a new level. In recent years, newly proposed algorithms [10, 12, 20, 24, 37, 41, 51] for point cloud semantic segmentation have predominantly leveraged deep learning techniques. In these noteworthy works, some focus on data augmentation strategies during training for input point clouds, such as PointNeXT [32] and Mix3D [28]. Meanwhile, PointNet++ [31], PointCNN [22], PointConv [49], PTv1 [57], and PTv2 [50] achieve performance gains by improving the network structure. PointNet [30] initially introduced a deep learning architecture for handling unordered point cloud data. PointNet++ [31] introduced hierarchical network architecture; PointCNN [22] and PointConv [49] introduced convolutional operations; PTv1 [57] introduced self-attention mechanisms. Additionally, there are studies that lean towards specific application scenarios [20, 41, 51, 53] or different training paradigms [52, 55, 58].

Class imbalance. The class imbalance problem refers to the situation where there is a significant disparity in the number of samples among different categories. This imbalance will adversely affect the performance of neural networks [56]. To address the class imbalance problem in deep learning, various techniques and strategies have been proposed, including resampling [3, 13, 26, 33, 59], weighted loss functions [2, 8, 23, 38], generative methods [34, 47], transfer learning [25, 54], and re-calibration [29, 45]. Due to the complexity and sparsity of point clouds, the above mentioned methods can hardly address class imbalance issues in point cloud semantic segmentation.

Category prototype. In few-shot learning [19, 35, 39, 40, 46], prototypes are often utilized as representatives of categories with limited training samples, aiding in the generalization to new instances or unseen categories with few examples. These prototypes can be used to measure the similarity between query instances and support instances belonging to different categories, enabling effective classification or regression. In weakly-supervised learning [4, 9, 21, 52, 55], prototypes can be employed to represent latent structures or concepts within the data, guiding the learning process in the absence of precise labels or annotations. In both few-shot and semi-supervised learning, the problems are addressed within fixed training and testing paradigms. However, minority category prototypes still tend to be influenced by prototypes of other categories, thereby leaving the issue of class imbalance unresolved.

3 Motivation

A typical point cloud semantic segmentation network consists of a representation and a classifier, as shown in Fig. 2. The representation maps the input point cloud to a high-dimensional feature space, and then the features are classified by the classifier. Tab. 1 and Fig. 3 illustrate the relationships between feature centers of different point subsets in the feature space of the PTv1, which is trained and tested on the S3DIS dataset [1]. The feature centers of TP points in the training set and test set are closely aligned, while the feature centers of FN

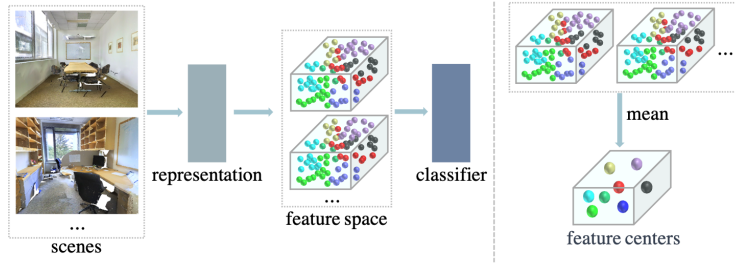


Fig. 2: The general process of point cloud semantic segmentation networks (including PointNet++ [31], PTV1 [57], PTV2 [50], RandLANet [15], KPConv [44], etc.).

Table 1: The cosine similarity between the feature centers of TP (True Positive), FP (False Positive), and FN (False Negative) subsets in the test set and the feature center of the TP subset in the training set.

Category	ceiling	floor	wall	column	window	door	table	chair	sofa	bookcase	board	clutter
TP	1.00	1.00	1.00	1.00	1.00	1.00	1.00	1.00	1.00	1.00	1.00	1.00
FP	0.94	0.94	0.98	0.98	0.97	0.97	0.98	0.97	0.93	0.99	0.97	0.99
FN	0.55	0.64	0.78	0.75	0.74	0.78	0.78	0.75	0.81	0.82	0.85	0.81

points in the test set are obviously different from those of TP points. In Fig. 4, when some point features are far away from the feature centers, they may be misclassified. Furthermore, we validated through experiments that PointNet++, PTV2, RandLANet, and KPConv exhibit similar phenomenon in their feature spaces.

Therefore, the reason why point cloud segmentation networks can correctly understand scenes is that they project the point cloud with complex textures and spatial information into the vicinity of corresponding feature prototypes in the metric space as shown in Fig. 1. The discriminative prototypes for minority categories and small intra-class variance will lead to better performance on minority categories. So how to effectively obtain and utilize high-quality prototypes for minority categories becomes the key issues in this study.

4 Methodology

The overview of the proposed method **SPG** is shown in Fig. 5. **SPG** consists of a dual-branch structure, with the main branch being the mainstream segmentation network such as PointNet++, PTV1, PTV2, and the auxiliary branch comprising the encoder from the segmentation network along with a projection head. The details of **SPG** will be introduced in this section, including how to extract feature prototypes of point clouds by the auxiliary branch, how to utilize the prototypes to supervise the main segmentation network and how to align the convergence direction of the two branches. Suppose that \mathbf{X} is the point set of current scene. The task of **SPG** is to assign a per point label to each member of \mathbf{X} , which will

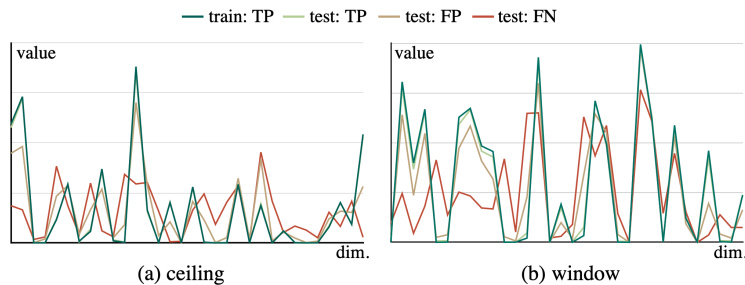


Fig. 3: The values of feature centers of "ceiling" and "window" in each dimension.

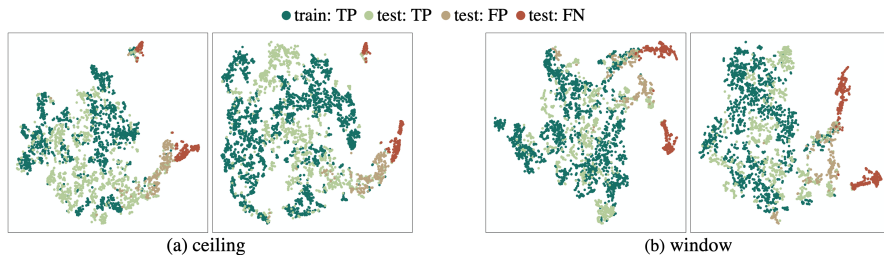


Fig. 4: The feature distributions of "ceiling" and "window". They are visualized by t-SNE [27].

be realized by the main branch. Hence, **SPG** only requires the main branch to infer the point cloud, and it does not introduce any additional computational complexity compared to the base network. **SPG** allows various choices of the base network without any constraints.

4.1 Point Cloud Prototype Extraction

The category prototype extraction places a stronger emphasis on the intrinsic characteristics of different point categories. To avoid introducing interference from heterogeneous features when the encoder aggregates neighborhood information, the point cloud \mathbf{X} of whole scene is separated into several point sets $\{\mathbf{X}_1, \dots, \mathbf{X}_c, \dots, \mathbf{X}_C\}$ by category labels, where the subscript c refers to category c and the capital C represents the number of categories. Subsequently, these point sets are input into the auxiliary branch network, which is composed of the encoder $f_e(\cdot)$ from the base segmentation network and a projection head $f_p(\cdot)$. The projection head is a multi-layer perceptron (MLP) with one hidden layer.

The high-dimensional abstract feature set \mathbf{H}_c of category c are extracted by the encoder $f_e(\cdot)$, which could be formalized as:

$$\mathbf{H}_c = f_e(\mathbf{X}_c). \quad (1)$$

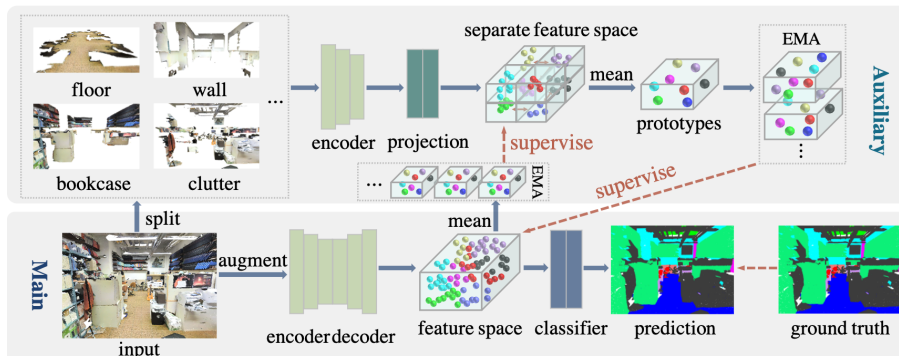


Fig. 5: The overall framework of **SPG**. The grouped point sets are projected into separate feature subspaces via a plug-and-play auxiliary branch, facilitating the derivation of discriminative prototypes. The feature prototypes of the current scene, in combination with those from historical scenes, provide supervision for the feature space of the main branch to reduce the intra-class variance. Simultaneously, the features correctly classified by the main branch also supervise the feature space of the auxiliary branch, ensuring their convergence aligning with each other.

Then, the projection head is used to map the high-dimensional abstract feature $\mathbf{h}_{c,i} \in \mathbf{H}_c$ to the space \mathcal{S}_c where the corresponding category prototype is extracted, where i means the feature index. The projection head is a multi-layer perceptron (MLP) with one or two hidden layers depending on the feature dimension. The MLP with one hidden layer can be expressed by the following equation:

$$\mathbf{f}_{c,i} = L_2(\sigma^{(2)}(W^{(2)}\sigma^{(1)}(W^{(1)}\mathbf{h}_{c,i}))), \quad (2)$$

where $L_2(\cdot)$ denotes L_2 normalization; $\sigma^{(1)}$ and $\sigma^{(2)}$ are the ReLU nonlinearities; $W^{(1)}$ and $W^{(2)}$ are the weight of linear layers. A supervised contrastive loss L_{con} between point features is employed to enhance the discrimination of features from different categories.

$$L_{con} = \sum_{c=1}^C \frac{-1}{N_c - 1} \sum_{i=1}^{N_c} \sum_{p \in P(i)} \log \frac{\exp(\mathbf{f}_{c,i} \cdot \mathbf{f}_{c,p}/\tau)}{\sum_{a \in A(i)} \exp(\mathbf{f}_{c,i} \cdot \mathbf{f}_a/\tau)}, \quad (3)$$

where N and N_c refer to the number of features in separate space \mathcal{S}_c and entire space \mathcal{S} , respectively; τ is the scalar temperature parameter whose default value is 0.07; $A(i) \equiv \{1, 2, \dots, N\} \setminus \{i\}$, and $P(i) \equiv \{1, 2, \dots, N_c\} \setminus \{i\}$. It furnishes a portion of the backpropagation gradient for updating the auxiliary branch network, and the other portion is supplied by prototype supervision from the feature space of main branch, which is depicted in Fig. 5.

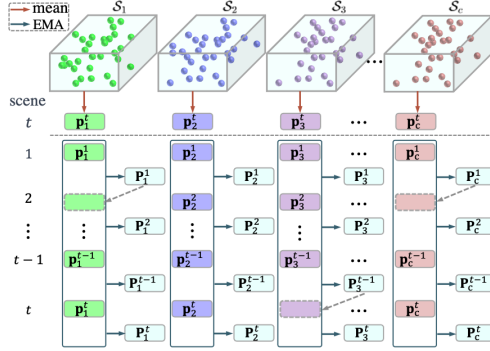


Fig. 6: The extraction of prototypes from separate feature subspaces and the EMA process. If there is no point set for category c in the current scene t , its prototype is assigned with the EMA of the prototypes from previous $t - 1$ scenes.

Fig. 6 illustrates the extracting process of prototypes $\{\mathbf{P}_1^t, \mathbf{P}_2^t, \dots, \mathbf{P}_c^t\}$ from separate feature subspaces $\{\mathcal{S}_1, \mathcal{S}_2, \dots, \mathcal{S}_c\}$ in the auxiliary. The prototype \mathbf{p}_c^t of the current scene t for category c in the feature subspace \mathcal{S}_c is obtained by taking the mean of normalized features of category c , which could be formalized as:

$$\mathbf{p}_c^t = \frac{1}{N_c} \sum_{i=1}^{N_c} \mathbf{f}_{c,i}^t. \quad (4)$$

In order to ensure that the prototypes extracted by the auxiliary branch contain not only the semantic information of current scene but also the collective semantic information from all training scenes, exponential moving average (EMA) is applied to obtain the prototypes:

$$\mathbf{P}_c^t = (1 - \alpha)\mathbf{p}_c^t + \alpha\mathbf{P}_c^{t-1}, \quad (5)$$

where the parameter α represents the smoothing factor, controlling the weight of the new observation \mathbf{p}_c^t in calculating \mathbf{P}_c^t .

4.2 Consistency Constraint for Convergence

The input X is processed through the encoder $f_e'(\cdot)$ and decoder $f_d'(\cdot)$ of the main branch to obtain the feature set \mathbf{H}' :

$$\mathbf{H}' = f_d'(f_e'(\mathbf{X})). \quad (6)$$

The discriminative prototypes $\{\mathbf{P}_1, \mathbf{P}_2, \dots, \mathbf{P}_c\}$, which is obtained from the separate feature subspaces in the auxiliary branch, are used to guide the distribution of \mathbf{H}' . This process can be formalized as follows:

$$L'_{t1} = \frac{1}{N'} \sum_{c=1}^C \sum_{i \in \mathcal{P}(c)} \text{smooth}_{L1}(L_2(\mathbf{h}'_i) - \mathbf{P}_c), \quad (7)$$

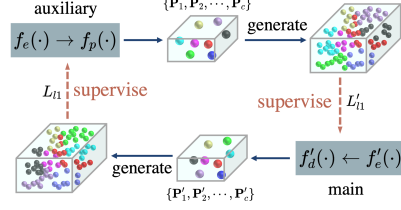


Fig. 7: Interaction loop between the auxiliary branch and the main branch. The two branches use their respective prototypes to generate features for mutual supervision, transferring cognitive prototype knowledge.

in which

$$\text{smooth}_{L_1}(x) = \begin{cases} 0.5x^2 & \text{if } |x| < 1, \\ |x| - 0.5 & \text{otherwise.} \end{cases} \quad (8)$$

Here, N' is the number of features in \mathbf{H}' ; $\mathcal{P}(c)$ refers to the index set of the feature subset that belongs to category c ; \mathbf{h}'_i is the i -th feature in \mathbf{H}' .

The loss L'_{l1} in Eq. (7) and cross-entropy loss L'_{ce} jointly provides the back-propagation gradient for the update of the segmentation network in main branch. The cross-entropy loss is expressed as follows:

$$L'_{ce} = -\frac{1}{N'} \sum_{i=1}^{N'} y_i \log(f_c(\mathbf{h}'_i)), \quad (9)$$

where $f_c(\cdot)$ represents the classifier and y_i is the ground truth label for the i -th point.

As shown in Fig. 7, **SPG** not only employs the feature prototypes of auxiliary branch to constrain the feature space of main branch (Eq. (7)), but also utilizes the feature prototypes of main branch to constrain the feature space of auxiliary branch for the consistent convergence between the main branch and the auxiliary branch. The loss L_{l1} in Fig. 7 could be expressed as:

$$L_{l1} = \frac{1}{N} \sum_{c=1}^C \sum_{i \in \mathcal{P}'(c)} \text{smooth}_{L_1}(\mathbf{f}_{c,i} - \mathbf{P}'_c), \quad (10)$$

where $\mathcal{P}'(c)$ refers to the index set of the features in \mathcal{S}_c . The prototypes of main branch, denoted as $\{\mathbf{P}'_1, \mathbf{P}'_2, \dots, \mathbf{P}'_c\}$, are extracted from the feature sets $\{\mathbf{H}'^1, \mathbf{H}'^2, \dots, \mathbf{H}'^t\}$ in the same manner as described in Eq. (4) and Eq. (5). To ensure feature accuracy, only features that are classified correctly are selected from \mathbf{H}' to participate in prototype computation.

Since the two branches of the **SPG** framework are trained simultaneously online, the overall loss is simply the sum of the losses from Eq. (3), Eq. (10), Eq. (7) and Eq. (9). This does not introduce complex training strategies, and it is represented as follows:

$$L = w_1 L_{con} + w_2 L_{l1} + w_3 L'_{l1} + w_4 L'_{ce}, \quad (11)$$

where w_1 , w_2 , w_3 and w_4 are the loss weights and their default values are 1.

5 Experiment

The experimental evaluations are conducted on four public benchmark datasets, S3DIS [1], ScanNet v2 [7], ScanNet200 [36] and Toronto-3D [42], and the collected real-world data. The effectiveness of the proposed method are validated through relevant experiments. The real-world data is outdoor point cloud with color information, collected by **Livox Horizon LiDAR** and fused with RGB images.

5.1 Data and Metric

All of these four publicly available datasets have been widely used to evaluate the performance of 3D semantic segmentation algorithms. S3DIS consists of point clouds captured from 6 areas with detailed annotations for 13 semantic categories. ScanNet v2 provides 1513 RGB-D scans of various scenes with per-point semantic labels for 20 categories, in which 1201 scenes are used for training and 312 for validation. ScanNet200 consists of 200 categories, an order of magnitude more than previous. Toronto-3D covers 1km of streets and consists of about 78.3 million points, which is divided into four sections. The second section is used for validation and the rest sections for training. For evaluating the performance of the proposed method on S3DIS area5, the metrics of mean class-wise intersection over union (mIoU), mean of class-wise accuracy (mAcc), and overall point-wise accuracy (OA) are utilized. Following a standard protocol [31, 50], mIoU is employed as the evaluation metric for assessing the performance on the validation set of ScanNet v2 and ScanNet200. Toronto-3D adopts the metrics of mIoU and OA.

Table 2: Semantic segmentation performance on S3DIS Area5, ScanNet v2, ScanNet200 and Toronto-3D.

Method	input Params.(M)		S3DIS Area5			ScanNet v2	ScanNet200	Toronto-3D	
			OA	mACC	mIoU	mIoU	mIoU	OA	mIoU
PointCNN [22]	point	0.6	85.9	63.9	57.3	-	-	-	-
DGCNN [48]	point	1.3	83.6	-	57.9	-	-	94.2	61.8
PointConv [49]	point	-	-	67.0	58.3	61.0	-	-	-
KPConv [44]	point	15.0	-	72.8	67.1	69.2	-	95.4	69.1
SparseConvNet [11]	voxel	-	-	-	-	69.3	-	-	-
MinkowskiNet [6]	voxel	-	-	71.7	65.4	72.1	25.0	-	-
CBL [43]	point	18.6	90.6	75.2	69.4	-	-	-	-
PointNetXt [32]	point	41.6	90.6	76.8	70.5	-	-	-	-
Stratified Transformer [18]	point	8.0	91.5	78.1	72.0	74.3	-	-	-
PointNet++ [31]	point	1.0	83.0	-	53.5	53.5	-	92.6	59.5
SPG(PointNet++)	point	1.0	87.6 (↑4.6)	70.8 (↑11.5)	64.0 (↑11.5)	55.8 (↑2.3)	-	93.8 (↑1.2)	61.2 (↑1.7)
PTv1 [57]	point	7.8	90.8	76.5	70.4	70.6	27.8	96.1	78.8
SPG(PTv1)	point	7.8	91.2 (↑0.4)	77.9 (↑1.4)	71.5 (↑1.1)	71.3 (↑0.7)	29.1 (↑1.3)	96.7 (↑0.6)	80.0 (↑1.2)
PTv2 [50]	point	3.9/11.3	91.1	77.9	71.6	75.4	30.2	97.2	81.6
SPG(PTv2)	point	3.9/11.3	91.9 (↑0.8)	79.5 (↑1.6)	73.3 (↑1.7)	76.0 (↑0.6)	31.5 (↑1.3)	97.6 (↑0.4)	83.1 (↑1.5)

5.2 Performance Comparison

It is evident that **SPG** significantly improves the performance of base segmentation networks (*i.e.*, PointNet++, PTv1, PTv2) on the four benchmark datasets, as shown in Tab. 2. On S3DIS area5, the OA, mAcc, and mIoU metrics for PointNet++ are improved by 4.6% and 11.5%; the OA, mAcc, and mIoU metrics for PTv1 are improved by 0.4%, 1.4% and 1.1%; and the three metrics for PTv2 have been elevated to the state-of-the-art (SOTA) levels, achieving values of 91.9%, 79.5%, and 73.3%, respectively. On the ScanNet v2, the mIoU for the

Table 3: Semantic segmentation performance of each category on S3DIS Area5.

Category	ceiling	floor	wall	beam	column	window	door	table	chair	sofa	bookcase	board	clutter	mIoU
Train(%)	19.14	16.51	27.25	2.42	2.13	2.12	5.48	3.24	4.07	0.49	4.71	1.26	11.19	
Test(%)	19.57	16.54	29.20	0.03	1.76	3.52	3.03	3.75	1.87	0.27	10.35	1.19	8.92	
PointNet [30]	88.8	97.3	69.8	0.1	3.9	46.3	10.8	59.0	52.6	5.9	40.3	26.4	33.2	41.1
PointCNN [22]	92.3	98.2	79.4	0.0	17.6	22.8	62.1	74.4	80.6	31.7	66.7	62.1	56.7	57.3
KPCConv [44]	92.8	97.3	82.4	0.0	23.9	58.0	69.0	81.5	91.0	75.4	75.3	66.7	58.9	67.1
CBL [43]	93.9	98.4	84.2	0.0	37.0	57.7	71.9	91.7	81.8	77.8	75.6	69.1	62.9	69.4
PointNeXt [32]	94.2	98.5	84.4	0.0	37.7	59.3	74.0	83.1	91.6	77.4	77.2	78.8	60.6	70.5
PTv1 [57]	94.0	98.5	86.3	0.0	38.0	63.4	74.3	89.1	82.4	74.3	80.2	76.0	59.3	70.4
SPG(PTv1)	95.0	98.0	87.0	0.0	44.8	63.0	73.9	83.3	91.0	77.2	77.4	76.9	61.6	71.5
	(↑1.0)	(↓0.5)	(↓0.7)	(-)	(↑6.8)	(↓0.4)	(↓0.4)	(↓5.8)	(↑8.6)	(↑2.9)	(↓2.8)	(↑0.9)	(↑1.3)	(↑1.1)
PTv2 [50]	95.2	98.7	86.1	0.0	38.9	61.8	72.5	83.9	92.5	75.7	77.9	83.9	63.6	71.6
SPG(PTv2)	95.1	98.7	86.9	0.0	38.9	64.6	78.0	85.2	92.7	83.0	79.5	85.1	65.0	73.3
	(↓0.1)	(-)	(↑0.8)	(-)	(-)	(↑2.8)	(↑5.5)	(↑1.3)	(↑0.2)	(↑7.3)	(↑1.6)	(↑1.2)	(↑1.4)	(↑1.7)

Table 4: Segmentation performance of each category on Toronto-3D

Category	Road	Road marking	Natural	Building	Utility line	Pole	Car	Fence	mIoU
Train(%)	42.57	1.69	20.63	24.50	1.35	1.57	6.78	0.90	
Test(%)	63.13	2.97	19.24	8.85	0.85	1.54	3.23	0.18	
PointNet++ [31]	92.9	0.0	86.1	82.2	61.0	62.8	76.4	14.4	59.5
DGCNN [48]	93.9	0.0	91.3	80.4	62.4	62.3	88.3	15.8	61.8
KPCConv [44]	94.6	0.1	96.1	91.5	87.7	81.6	85.7	15.7	69.1
MS-TGNet [42]	94.4	17.2	95.7	88.8	76.0	74.0	94.2	23.6	70.5
PTv1 [57]	92.9	59.6	96.7	91.9	80.6	77.4	89.1	42.2	78.8
SPG(PTv1)	94.0(↑1.1)	63.3(↑3.7)	96.7(-)	92.4(↑0.5)	82.7(↑2.1)	79.3(↑1.9)	89.2(↑0.1)	42.4(↑0.2)	80.0
PTv2 [50]	96.6	72.4	96.9	91.8	86.0	81.4	90.6	37.3	81.6
SPG(PTv2)	96.7(↑0.1)	73.8(↑1.4)	97.0(↑0.1)	93.4(↑1.6)	86.4(↑0.4)	81.7(↑0.3)	90.9(↑0.3)	45.1(↑7.8)	83.1

three networks has shown respective improvements of 2.3%, 0.7%, and 0.6%. On the ScanNet200 dataset with a larger number of categories, **SPG** can also help PTv1 and PTv2 achieve better segmentation performance with a mIoU increase of 1.3%. On the outdoor dataset Toronto-3D, **SPG** can increase the mIoU of PTv1 and PTv2 to more than 80%, with the latter achieving the top performance on this dataset. The experiments conducted on various datasets with different base networks confirm the strong generalization capability of **SPG**. Furthermore, this method does not make any modifications to the base segmentation networks during the inference process. So the inference speed of the improved networks will keep the same as the base networks despite the significant increase in performance.

The first two rows in Tab. 3 and Tab. 4 refer to the proportions of samples for each category in the training and test datasets, which are measured in terms of the number of points. It can be observed that the segmentation networks exhibit superior performance for the "ceiling", "floor", and "wall" categories on S3DIS and "Road", "Natural", and "Building" categories on Toronto-3D, which have larger sample size. However, the segmentation performance for minority categories is relatively lower. **SPG** can enhance the segmentation performance of different categories, especially demonstrating more pronounced effects on minority categories.

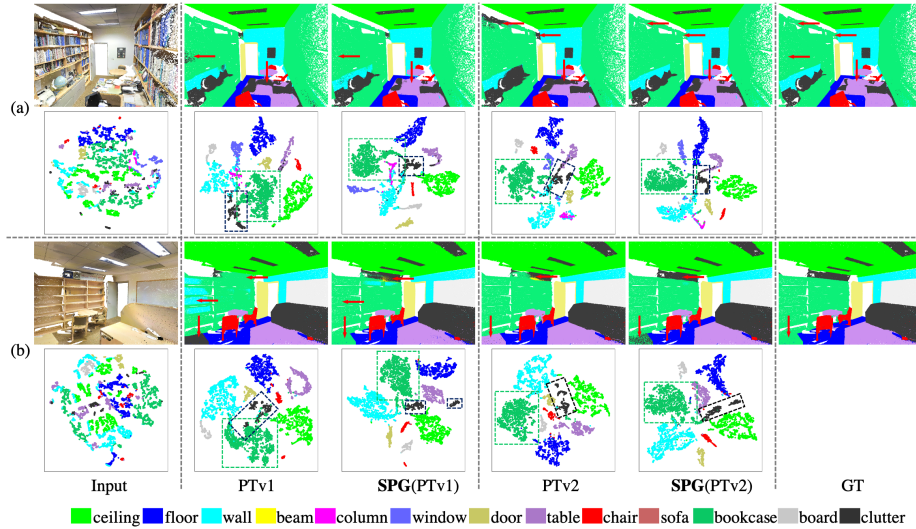


Fig. 8: Visualization of segmentation results and feature distributions on two scenes in S3DIS Area5. The maps below segmentation results are their corresponding feature distributions. As shown in Fig. 2, the first row in (a) and (b) is the visualization of the output segmentation results, and the second row is the visualization of the feature distributions after the representation.

Table 5: The performance of different balancing methods on S3DIS Area5.

Method	Base Focal [23]	Weighted CE [2]	BNN [59]	Meta-Softmax [33]	NORCAL [29]	SPG	
PTv1 [57]	70.4	69.2 (↓1.2)	69.6 (↓0.8)	69.3 (↓1.1)	69.8 (↓0.6)	69.9 (↓0.5)	71.5 (↑1.1)
PTv2 [50]	71.6	70.7 (↓0.9)	70.9 (↓0.7)	-	-	-	73.3 (↑1.7)

Separate	L_{con}	L_{l1}	L'_{l1}	L'_{ce}	mIoU
✓	✓	✓	✓	✓	73.3
✓	✓	✓	✓	✓	72.2(↓1.1)
✓	✓	✓	✓	✓	72.6(↓0.7)
✓	✓	✓	✓	✓	72.8(↓0.5)
✓	✓	✓	✓	✓	71.6(↓1.7)

Table 6: Ablation study of SPG(PTv2) on S3DIS Area5. "Separate" refers to whether to use the separate subspaces in the auxiliary branch.

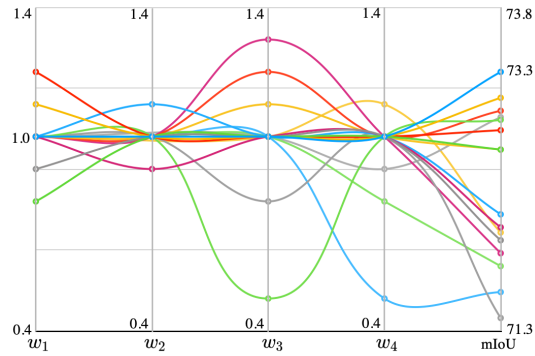


Fig. 11: Loss weight adjustment in Eq. (11) on S3DIS Area5.

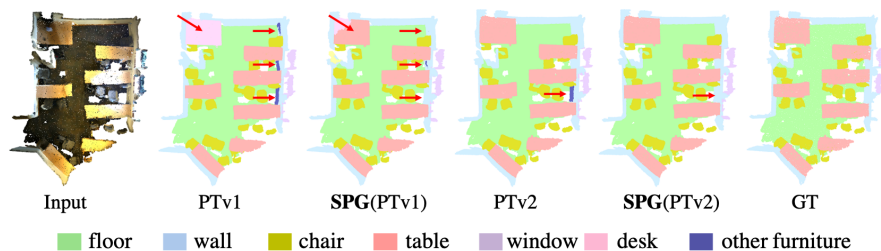


Fig. 9: Visualization of segmentation results on ScanNet v2. The red arrows point to notable areas.

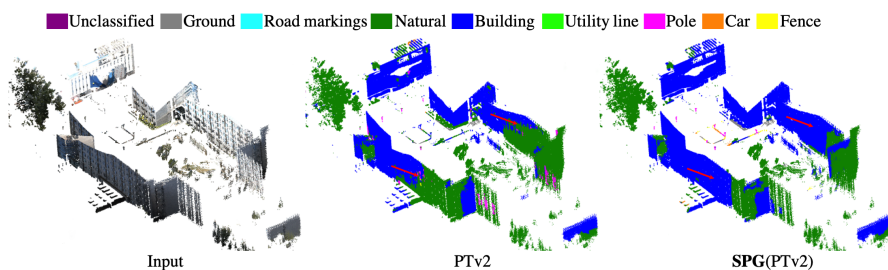


Fig. 10: Qualitative results of the real-world data. The main part of the point cloud consists of buildings, with some trees surrounding them.

5.3 Qualitative Results

Fig. 8 displays the improvements on the segmentation performance of PTv1 and PTv2 due to the training guidance from **SPG**, and the corresponding feature distribution maps. In scene (a), due to the proximity of "bookcase" and "clutter" category in the feature spaces of PTv1 and PTv2 (indicated within the grass green and black rectangle), the "bookcase" points (indicated by red arrows) are misclassified as "clutter" points. For the same reason, "table" points are also misclassified as "clutter" points. After training with **SPG** guidance, the features of "bookcase" and "table" categories become more discriminative, significantly reducing the probability of misclassification. In scene (b), the networks trained without **SPG** guidance exhibit limited discrimination for the "bookcase" and "clutter" categories in the feature space. This reduced cohesion makes it more susceptible to be misclassified. In the scene shown in Fig. 9, which is from ScanNet v2, it is also evident that **SPG** can assist the segmentation network in achieving improved segmentation results.

We test the models that are pretrained on Toronto-3D on the real-world collected data, and the qualitative results are shown in Fig. 10. It can be observed that **SPG** demonstrates significant advantages in handling real-world data. By assisting the base segmentation network in reducing intra-class feature distances and increasing inter-class distances, **SPG** markedly reduces the probability of

Table 7: Hyperparameter tuning on S3DIS Area5. t represents the number of iterations in each training epoch.(a) τ denotes the temperature in Eq. (3).

τ	0.02	0.05	0.06	0.07	0.08	0.10
mIoU	72.2	73.0	72.9	73.3	72.9	72.0

(b) α is the smoothing factor in Eq. (5).

α	0.9	0.99	0.999	1-1/t	1-1/ $\frac{t}{2}$	1-1/ $\frac{t}{10}$
mIoU	72.1	72.6	73.0	73.3	72.8	72.3

misclassifying point clouds belonging to the "Building" category as "Natural" and "Pole" categories.

5.4 Ablation and Hyperparameters

Point cloud semantic segmentation lacks clear sample statistics (*e.g.*, images in classification, boxes in object detection), making methods [2, 29, 33] that depend on statistical priors challenging to work. Additionally, resampling data [33, 59] will disrupt the global semantics and context information of the input point cloud and re-weighting per-pixel/point loss [2, 23] may cause gradient issues during optimization. The proposed method, **SPG**, does not rely on statistical priors, resampling samples, or point-wise loss adjustments, thus avoiding potential performance degradation of other methods in Tab. 5. From the ablation experiments in Tab. 6, it can be observed that prototypes extracted from separate feature subspaces can more effectively guide the training of segmentation networks, resulting in superior segmentation performance. The loss constraints of each component in Eq. (11) are beneficial to the improvement of performance.

As shown in Fig. 11, when w_1 , w_2 , w_3 , and w_4 are all set to their default value of 1, **SPG** (PTv2) achieves the best performance. This suggests that the losses of each part are balanced without the need for complex adjustments. In Tab. 7, **SPG**(PTv2) achieves the best performance at the temperature $\tau=0.07$ and the smoothing factor $\alpha=1-1/t$. The above hyperparameter settings can be transferred to different base networks (*e.g.*, PointNet++, PTv1) to achieve the segmentation performance shown in Tab. 2 on various datasets.

6 Conclusion

This study attempts to address the issue of class imbalance in point cloud semantic segmentation from the perspective of point cloud feature prototypes and proposes a targeted solution called **SPG**. **SPG** extracts prototypes from separate feature subspaces to guide the training of segmentation network. This process makes the distribution of homogeneous features more similar and the distribution of heterogeneous features more different, which effectively mitigates the cognitive bias introduced by class imbalance. Extensive experiments conducted on different networks and datasets confirm the effectiveness of **SPG** in enhancing the discrimination of minority category features, ultimately improving overall segmentation accuracy.

Acknowledgements

It is sponsored by State Key Laboratory of Intelligent Green Vehicle and Mobility under Project No. KFY2416. Thanks to Prof. Wenguang Wang of Beihang University for providing the collected real-world data.

References

1. Armeni, I., Sener, O., Zamir, A.R., Jiang, H., Brilakis, I., Fischer, M., Savarese, S.: 3d semantic parsing of large-scale indoor spaces. In: Proceedings of the IEEE/CVF Conference on Computer Vision and Pattern Recognition. pp. 1534–1543 (2016) [4](#), [9](#)
2. Aurelio, Y.S., De Almeida, G.M., de Castro, C.L., Braga, A.P.: Learning from imbalanced data sets with weighted cross-entropy function. *Neural Processing Letters* **50**, 1937–1949 (2019) [2](#), [4](#), [12](#), [14](#)
3. Chawla, N.V., Bowyer, K.W., Hall, L.O., Kegelmeyer, W.P.: Smote: synthetic minority over-sampling technique. *Journal of Artificial Intelligence Research* **16**, 321–357 (2002) [2](#), [4](#)
4. Chen, Q., Yang, L., Lai, J.H., Xie, X.: Self-supervised image-specific prototype exploration for weakly supervised semantic segmentation. In: Proceedings of the IEEE/CVF Conference on Computer Vision and Pattern Recognition. pp. 4288–4298 (2022) [4](#)
5. Chen, X., Fan, H., Girshick, R., He, K.: Improved baselines with momentum contrastive learning. *arXiv preprint arXiv:2003.04297* (2020) [3](#)
6. Choy, C., Gwak, J., Savarese, S.: 4d spatio-temporal convnets: Minkowski convolutional neural networks. In: Proceedings of the IEEE/CVF Conference on Computer Vision and Pattern Recognition. pp. 3075–3084 (2019) [10](#)
7. Dai, A., Chang, A.X., Savva, M., Halber, M., Funkhouser, T., Nießner, M.: ScanNet: Richly-annotated 3d reconstructions of indoor scenes. In: Proceedings of the IEEE/CVF Conference on Computer Vision and Pattern Recognition. pp. 5828–5839 (2017) [9](#)
8. Dong, Q., Gong, S., Zhu, X.: Imbalanced deep learning by minority class incremental rectification. *IEEE Transactions on Pattern Analysis and Machine Intelligence* **41**(6), 1367–1381 (2018) [4](#)
9. Du, Y., Fu, Z., Liu, Q., Wang, Y.: Weakly supervised semantic segmentation by pixel-to-prototype contrast. In: Proceedings of the IEEE/CVF Conference on Computer Vision and Pattern Recognition. pp. 4320–4329 (2022) [4](#)
10. Feng, T., Wang, W., Wang, X., Yang, Y., Zheng, Q.: Clustering based point cloud representation learning for 3d analysis. In: Proceedings of the IEEE/CVF International Conference on Computer Vision. pp. 8283–8294 (2023) [4](#)
11. Graham, B., Engelcke, M., Van Der Maaten, L.: 3d semantic segmentation with submanifold sparse convolutional networks. In: Proceedings of the IEEE/CVF Conference on Computer Vision and Pattern Recognition. pp. 9224–9232 (2018) [10](#)
12. Han, J., Liu, K., Li, W., Chen, G., Wang, W., Zhang, F.: A large-scale network construction and lightweighting method for point cloud semantic segmentation. *IEEE Transactions on Image Processing* **33**, 2004–2017 (2024) [1](#), [4](#)
13. He, H., Garcia, E.A.: Learning from imbalanced data. *IEEE Transactions on Knowledge and Data Engineering* **21**(9), 1263–1284 (2009) [4](#)

14. He, K., Fan, H., Wu, Y., Xie, S., Girshick, R.: Momentum contrast for unsupervised visual representation learning. In: Proceedings of the IEEE/CVF Conference on Computer Vision and Pattern Recognition. pp. 9729–9738 (2020) [3](#)
15. Hu, Q., Yang, B., Xie, L., Rosa, S., Guo, Y., Wang, Z., Trigoni, N., Markham, A.: Randla-net: Efficient semantic segmentation of large-scale point clouds. In: Proceedings of the IEEE/CVF Conference on Computer Vision and Pattern Recognition. pp. 11108–11117 (2020) [5](#)
16. Kang, B., Xie, S., Rohrbach, M., Yan, Z., Gordo, A., Feng, J., Kalantidis, Y.: Decoupling representation and classifier for long-tailed recognition. In: Eighth International Conference on Learning Representations (ICLR) (2020) [2](#)
17. Khosla, P., Teterwak, P., Wang, C., Sarna, A., Tian, Y., Isola, P., Maschinot, A., Liu, C., Krishnan, D.: Supervised contrastive learning. *Advances in Neural Information Processing Systems* **33**, 18661–18673 (2020) [3](#)
18. Lai, X., Liu, J., Jiang, L., Wang, L., Zhao, H., Liu, S., Qi, X., Jia, J.: Stratified transformer for 3d point cloud segmentation. In: Proceedings of the IEEE/CVF Conference on Computer Vision and Pattern Recognition. pp. 8500–8509 (2022) [10](#)
19. Li, A., Luo, T., Xiang, T., Huang, W., Wang, L.: Few-shot learning with global class representations. In: Proceedings of the IEEE/CVF International Conference on Computer Vision. pp. 9715–9724 (2019) [4](#)
20. Li, J., Dai, H., Han, H., Ding, Y.: Mseg3d: Multi-modal 3d semantic segmentation for autonomous driving. In: Proceedings of the IEEE/CVF Conference on Computer Vision and Pattern Recognition. pp. 21694–21704 (2023) [4](#)
21. Li, J., Zhou, P., Xiong, C., Hoi, S.: Prototypical contrastive learning of unsupervised representations. In: International Conference on Learning Representations (2020) [4](#)
22. Li, Y., Bu, R., Sun, M., Wu, W., Di, X., Chen, B.: Pointcnn: Convolution on x-transformed points. *Advances in Neural Information Processing Systems* **31** (2018) [1](#), [3](#), [4](#), [10](#), [11](#)
23. Lin, T.Y., Goyal, P., Girshick, R., He, K., Dollár, P.: Focal loss for dense object detection. In: Proceedings of the IEEE/CVF International Conference on Computer Vision. pp. 2980–2988 (2017) [2](#), [4](#), [12](#), [14](#)
24. Liu, J., Chang, C., Liu, J., Wu, X., Ma, L., Qi, X.: Mars3d: A plug-and-play motion-aware model for semantic segmentation on multi-scan 3d point clouds. In: Proceedings of the IEEE/CVF Conference on Computer Vision and Pattern Recognition. pp. 9372–9381 (2023) [4](#)
25. Liu, J., Sun, Y., Han, C., Dou, Z., Li, W.: Deep representation learning on long-tailed data: A learnable embedding augmentation perspective. In: Proceedings of the IEEE/CVF Conference on Computer Vision and Pattern Recognition. pp. 2970–2979 (2020) [4](#)
26. Liu, X.Y., Wu, J., Zhou, Z.H.: Exploratory undersampling for class-imbalance learning. *IEEE Transactions on Systems, Man, and Cybernetics, Part B (Cybernetics)* **39**(2), 539–550 (2008) [2](#), [4](#)
27. Van der Maaten, L., Hinton, G.: Visualizing data using t-sne. *Journal of Machine Learning Research* **9**(11) (2008) [6](#)
28. Nekrasov, A., Schult, J., Litany, O., Leibe, B., Engelmann, F.: Mix3D: Out-of-Context Data Augmentation for 3D Scenes. In: International Conference on 3D Vision (3DV) (2021) [4](#)
29. Pan, T.Y., Zhang, C., Li, Y., Hu, H., Xuan, D., Changpinyo, S., Gong, B., Chao, W.L.: On model calibration for long-tailed object detection and instance segmen-

- tation. *Advances in Neural Information Processing Systems* **34**, 2529–2542 (2021) [4](#), [12](#), [14](#)
30. Qi, C.R., Su, H., Mo, K., Guibas, L.J.: Pointnet: Deep learning on point sets for 3d classification and segmentation. In: *Proceedings of the IEEE/CVF Conference on Computer Vision and Pattern Recognition*. pp. 652–660 (2017) [1](#), [3](#), [4](#), [11](#)
 31. Qi, C.R., Yi, L., Su, H., Guibas, L.J.: Pointnet++: Deep hierarchical feature learning on point sets in a metric space. *Advances in Neural Information Processing Systems* **30** (2017) [1](#), [3](#), [4](#), [5](#), [10](#), [11](#)
 32. Qian, G., Li, Y., Peng, H., Mai, J., Hammoud, H., Elhoseiny, M., Ghanem, B.: Pointnext: Revisiting pointnet++ with improved training and scaling strategies. *Advances in Neural Information Processing Systems* **35**, 23192–23204 (2022) [4](#), [10](#), [11](#)
 33. Ren, J., Yu, C., Ma, X., Zhao, H., Yi, S., et al.: Balanced meta-softmax for long-tailed visual recognition. *Advances in Neural Information Processing Systems* **33**, 4175–4186 (2020) [4](#), [12](#), [14](#)
 34. Ren, J., Liu, Y., Liu, J.: Ewgan: Entropy-based wasserstein gan for imbalanced learning. In: *Proceedings of the AAAI Conference on Artificial Intelligence*. vol. 33, pp. 10011–10012 (2019) [4](#)
 35. Ren, M., Triantafillou, E., Ravi, S., Snell, J., Swersky, K., Tenenbaum, J.B., Larochelle, H., Zemel, R.S.: Meta-learning for semi-supervised few-shot classification. *arXiv preprint arXiv:1803.00676* (2018) [4](#)
 36. Rozenberszki, D., Litany, O., Dai, A.: Language-grounded indoor 3d semantic segmentation in the wild. In: *European Conference on Computer Vision*. pp. 125–141. Springer (2022) [9](#)
 37. Saltori, C., Osep, A., Ricci, E., Leal-Taixé, L.: Walking your lidog: A journey through multiple domains for lidar semantic segmentation. In: *Proceedings of the IEEE/CVF International Conference on Computer Vision*. pp. 196–206 (2023) [4](#)
 38. Shu, J., Xie, Q., Yi, L., Zhao, Q., Zhou, S., Xu, Z., Meng, D.: Meta-weight-net: Learning an explicit mapping for sample weighting. *Advances in Neural Information Processing Systems* **32** (2019) [4](#)
 39. Snell, J., Swersky, K., Zemel, R.: Prototypical networks for few-shot learning. *Advances in Neural Information Processing Systems* **30** (2017) [2](#), [4](#)
 40. Sung, F., Yang, Y., Zhang, L., Xiang, T., Torr, P.H., Hospedales, T.M.: Learning to compare: Relation network for few-shot learning. In: *Proceedings of the IEEE/CVF Conference on Computer Vision and Pattern Recognition*. pp. 1199–1208 (2018) [4](#)
 41. Takmaz, A., Schult, J., Kaftan, I., Akçay, M., Leibe, B., Sumner, R., Engelmann, F., Tang, S.: 3d segmentation of humans in point clouds with synthetic data. In: *Proceedings of the IEEE/CVF International Conference on Computer Vision*. pp. 1292–1304 (2023) [4](#)
 42. Tan, W., Qin, N., Ma, L., Li, Y., Du, J., Cai, G., Yang, K., Li, J.: Toronto-3d: A large-scale mobile lidar dataset for semantic segmentation of urban roadways. In: *Proceedings of the IEEE/CVF Conference on Computer Vision and Pattern Recognition Workshops*. pp. 202–203 (2020) [9](#), [11](#)
 43. Tang, L., Zhan, Y., Chen, Z., Yu, B., Tao, D.: Contrastive boundary learning for point cloud segmentation. In: *Proceedings of the IEEE/CVF Conference on Computer Vision and Pattern Recognition*. pp. 8489–8499 (2022) [10](#), [11](#)
 44. Thomas, H., Qi, C.R., Deschaud, J.E., Marcotegui, B., Goulette, F., Guibas, L.J.: Kpconv: Flexible and deformable convolution for point clouds. In: *Proceedings of the IEEE/CVF International Conference on Computer Vision*. pp. 6411–6420 (2019) [3](#), [5](#), [10](#), [11](#)

45. Tian, J., Liu, Y.C., Glaser, N., Hsu, Y.C., Kira, Z.: Posterior re-calibration for imbalanced datasets. *Advances in Neural Information Processing Systems* **33**, 8101–8113 (2020) [4](#)
46. Vinyals, O., Blundell, C., Lillicrap, T., Wierstra, D., et al.: Matching networks for one shot learning. *Advances in Neural Information Processing Systems* **29** (2016) [4](#)
47. Wang, X., Lyu, Y., Jing, L.: Deep generative model for robust imbalance classification. In: *Proceedings of the IEEE/CVF Conference on Computer Vision and Pattern Recognition*. pp. 14124–14133 (2020) [4](#)
48. Wang, Y., Sun, Y., Liu, Z., Sarma, S.E., Bronstein, M.M., Solomon, J.M.: Dynamic graph cnn for learning on point clouds. *ACM Transactions on Graphics* **38**(5), 1–12 (2019) [10](#), [11](#)
49. Wu, W., Qi, Z., Fuxin, L.: Pointconv: Deep convolutional networks on 3d point clouds. In: *Proceedings of the IEEE/CVF Conference on Computer Vision and Pattern Recognition*. pp. 9621–9630 (2019) [1](#), [3](#), [4](#), [10](#)
50. Wu, X., Lao, Y., Jiang, L., Liu, X., Zhao, H.: Point transformer v2: Grouped vector attention and partition-based pooling. *Advances in Neural Information Processing Systems* **35**, 33330–33342 (2022) [3](#), [4](#), [5](#), [10](#), [11](#), [12](#)
51. Xiao, A., Huang, J., Xuan, W., Ren, R., Liu, K., Guan, D., El Saddik, A., Lu, S., Xing, E.P.: 3d semantic segmentation in the wild: Learning generalized models for adverse-condition point clouds. In: *Proceedings of the IEEE/CVF Conference on Computer Vision and Pattern Recognition*. pp. 9382–9392 (2023) [4](#)
52. Xu, X., Lee, G.H.: Weakly supervised semantic point cloud segmentation: Towards 10x fewer labels. In: *Proceedings of the IEEE/CVF Conference on Computer Vision and Pattern Recognition*. pp. 13706–13715 (2020) [2](#), [4](#)
53. Yan, X., Gao, J., Zheng, C., Zheng, C., Zhang, R., Cui, S., Li, Z.: 2dpass: 2d priors assisted semantic segmentation on lidar point clouds. In: *European Conference on Computer Vision*. pp. 677–695. Springer (2022) [4](#)
54. Yin, X., Yu, X., Sohn, K., Liu, X., Chandraker, M.: Feature transfer learning for face recognition with under-represented data. In: *Proceedings of the IEEE/CVF Conference on Computer Vision and Pattern Recognition*. pp. 5704–5713 (2019) [4](#)
55. Zhang, Y., Li, Z., Xie, Y., Qu, Y., Li, C., Mei, T.: Weakly supervised semantic segmentation for large-scale point cloud. In: *Proceedings of the AAAI Conference on Artificial Intelligence*. vol. 35, pp. 3421–3429 (2021) [2](#), [4](#)
56. Zhang, Y., Kang, B., Hooi, B., Yan, S., Feng, J.: Deep long-tailed learning: A survey. *IEEE Transactions on Pattern Analysis and Machine Intelligence* **45**(9), 10795–10816 (2023) [4](#)
57. Zhao, H., Jiang, L., Jia, J., Torr, P.H., Koltun, V.: Point transformer. In: *Proceedings of the IEEE/CVF International Conference on Computer Vision*. pp. 16259–16268 (2021) [1](#), [3](#), [4](#), [5](#), [10](#), [11](#), [12](#)
58. Zhao, N., Chua, T.S., Lee, G.H.: Few-shot 3d point cloud semantic segmentation. In: *Proceedings of the IEEE/CVF Conference on Computer Vision and Pattern Recognition*. pp. 8873–8882 (2021) [2](#), [4](#)
59. Zhou, B., Cui, Q., Wei, X.S., Chen, Z.M.: Bbn: Bilateral-branch network with cumulative learning for long-tailed visual recognition. In: *Proceedings of the IEEE/CVF Conference on Computer Vision and Pattern Recognition*. pp. 9719–9728 (2020) [4](#), [12](#), [14](#)